Processing Onboard Optical Data for Planetary Approach Navigation

CHARLES H. ACTON JR.*
Jet Propulsion Laboratory, Pasadena, Calif.

The Mariner 9 Spacecraft's science television camera provided an optical navigation experiment with TV pictures containing images of Mars' natural satellites and background stars. Required TV and spacecraft engineering data were extracted from the spacecraft telemetry stream and successfully processed in this near-real time experiment designed to validate the navigation content of spacecraft-based optical data. The preparation of this optical data for use in a navigation filter included development and calibration of a TV error model, identification of detected signals and estimation of the location of the center of each valid image, including associated statistics. Ground and in-flight calibrations allowed subsequent celestially referenced camera pointing knowledge of better than 6 arc sec. An average of 3.5 images per picture was found in the 19 pictures allotted the experiment during the 72 hr prior to Mars encounter. System performance was excellent, leading to very accurate trajectory estimates. The experiment provides a basis for the design of improved systems for future missions.

Introduction

CURRENT and projected Earth-based radio tracking techniques have been shown[1,2,3] to be marginal or inadequate for many future missions to the outer planets. The additional navigation accuracy required may be achieved within spacecraft design fuel-loading constraints by combining spacecraft-based optical measurements with Earth-based radio ranging and Doppler data during planetary approach. Images of the target planet's natural satellites against a background of stars may be used to obtain an estimate of the spacecraft trajectory substantially better and earlier than that available using only radio data,[4] allowing significant reductions in fuel requirements. The Mariner Mars 1971 mission provided a timely opportunity to test this optical navigation concept with real data. The objective of the optical navigation experiment was to formally demonstrate the navigational quality of optical data obtained from a TV camera and processed in a real mission environment.

Error Model

The extraction of data useful for navigation from the spacecraft telemetry stream and the rectification of this data for known errors are significant tasks leading to the development of optical observables suitable for use in a navigation filter. Intrinsic to this process is the formulation and calibration of spacecraft and sensor error models.

Images of Phobos, Deimos and stars were obtained from the narrow-angle science TV camera, the characteristics of which are listed in Table 1. The vidicon's active target raster of 9.6×12.5 mm is electronically scanned in 700 lines, and sampled at 832 picture elements (pixels) per scan line. The 500-mm focal length allows a $1.1 \times 1.4°$ field of view with an angular resolution of 6 arc sec. Each video sample is digitized to 9 bits (512 intensity levels) prior to transmission to Earth. A continuous, analytic error model developed for the camera[5] contains terms for symmetric and asymmetric radial and tangential distortion, electromagnetic and optical principle point null-offsets and scan coordinate system scale factor, nonorthogonality and rotation. The TV is hard mounted to a two-degree-of-freedom scan platform, with TV mounting misalignments, scan platform gimbal errors and misalignments, and pitch, yaw and roll sensor offsets and scale factor error comprising the remaining major components of the math model.

Table 1 Narrow angle camera characteristics

Field of view	$= 1.1 \times 1.4°$
Focal length	= 500 mm
Target dimensions	$= 9.6 \times 12.5$ mm
No. of scan lines	= 700
No. samples/line	= 832
Shutter speed	= Variable—6 millisec to 6.144 sec
Resolution	= 6 arc sec
Pixel size	$= 15\ \mu$
Scanning spot size	$= 25\ \mu$
Read out time	= 42 sec

Geometric ground calibration of the narrow-angle camera revealed electromagnetic distortion in both line and pixel directions, an example of which is shown in Fig. 1; optical distortion was found to be negligible. The electromagnet distortion calibration was effected by observing the position changes of reseau marks etched at known locations on the vidicon target. A preliminary light-transfer curve was developed for point sources by photographing stars with the prototype camera system. Signal level as a function of star magnitude[6] is shown in Fig. 2 for 2 values of limit cycle rate which bounded the expected spacecraft performance of about 20μ rad/sec. Each axis of the scan platform was individually ground-calibated to verify the associated math model and to serve a priori for in-flight calibration sequences.

An in-flight calibration of the camera and scan platform pointing system was performed 40 days prior to Mars encounter. Two sets of 31 pictures aimed at star clusters, single stars, Mars and Saturn provided a good set of data for redetermination of electromagnetic and optical distortion, vidicon light transfer and camera pointing in a flight environment. The first set of pictures was targeted at exceptionally bright

Presented as Paper 72-53 at the AIAA 10th Aerospace Sciences Meeting, San Diego, Calif., January 17–19, 1972; submitted February 16, 1972; revision received June 5, 1972. This research was supported under Contract NAS 7-100, sponsored by NASA. The author is indebted to W. G. Brackenridge, T. C. Duxbury, H. Ohtakay, and M. H. Bantell of the Jet Propulsion Lab. for their work on the experiment.

Index categories: Lunar and Planetary Trajectories; Spacecraft Navigation, Guidance, and Flight-Path Control Systems; Data Sensing and Presentation or Transmission Systems.

* Team Leader, Optical Navigation Measurements Group, MM'71, Navigation Team.

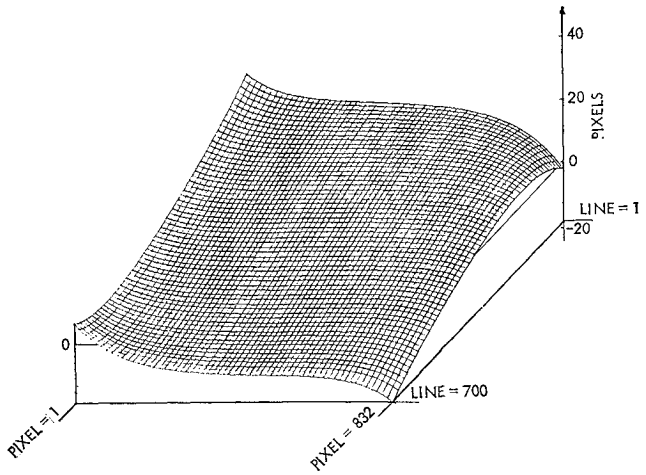

Fig. 1 Geometric distortion in pixel direction.

stars, Saturn, and a bright, compact star cluster to ensure acquision of an initial set of data independent of possible system degradation or bias during launch, maneuver, or cruise. These pictures indicated a 0.5° postlaunch pointing bias in one axis of the scan platform. A significant change of up to 6 pixels (36 arc sec) in the electromagnetic distortion, shown in Fig. 3, resulted from the absence of the Earth's magnetic field and possible movement of the vidicon beam deflection coils. Residual distortion, after fitting the continuous, analytic error model, resulted in a 1σ model error of 0.75 pixels with a maximum excursion of 1.8 pixels (Fig. 4). Images observed in three areas exhibiting particularly large residual distortion were either ignored or received additional correction using local linear interpolation.

Real time processing of video data resulted in detection of stars of magnitude 7.8, while nonreal time processing allowed detection of stars as dim as magnitude 9.3. Observed video intensity was seen to be a function of star magnitude, image location relative to scanning-beam geometry, and spacecraft attitude rate. Stars of magnitude 0.9 (Altair) and 8.6 are shown in Fig. 5 as three-dimensional plots to graphically represent the dynamic range of star image data.

The initial pointing recalibration and excellent vidicon sensitivity observed in the first set of pictures permitted some retargeting to optimize the second calibration set. Targets for these 31 pictures were selected to require camera pointing over the entire dynamic range of scan platform motion. Two or more star images were detected in 28 of these pictures, while a single image was observed in the remaining 4.

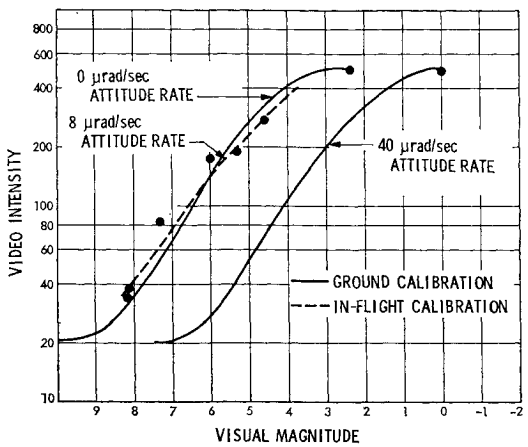

Fig. 2 Stellar light transfer curves.

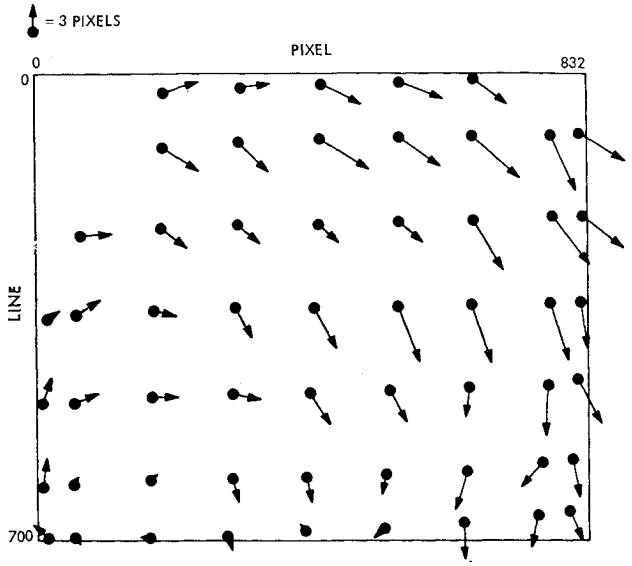

Fig. 3 Change in observed reseau locations.

Software Development

The ground-based software system performed picture planning, data extraction and data-rectification functions. Requirements to process a large volume of data from many sources in a short period of time using a heavily loaded time-sharing system indicated a need for simple, flexible, and highly automated computer programs. Picture planning entailed consideration of the spacecraft trajectory, Mars, Phobos and Deimos ephemerides, star locations (from the Smithsonian Star Catalogue), mission operations constraints, spacecraft limit cycle motion, and vidicon characteristics.

Planning included pictures of stars for calibration sequences, pictures of Phobos and Deimos against star backgrounds during Mars approach, and close-range pictures of Phobos and Deimos while in Mars orbit. An example of one form of graphic output from the planning program is shown in Fig. 6. This simulated TV picture, scaled to match the size of the mission-produced photographs, shows the expected locations of Phobos and eight stars with associated magnitudes in a picture taken at 14 hr before Mars encounter at a range of 176,752 km (Fig. 7). Offsets in the observed positions of the stars result from spacecraft limit cycle motion, while limit cycle, ephemeris error and trajectory error cause offsets in the observed position of Deimos. Each such a priori plot was regenerated after the associated picture was shuttered,

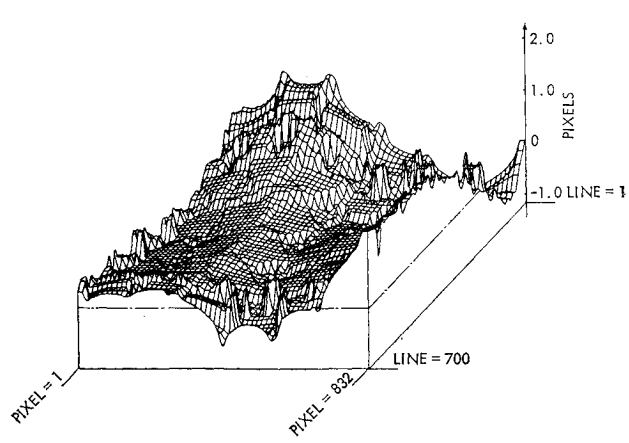

Fig. 4 Inflight TV calibration pixel residuals.

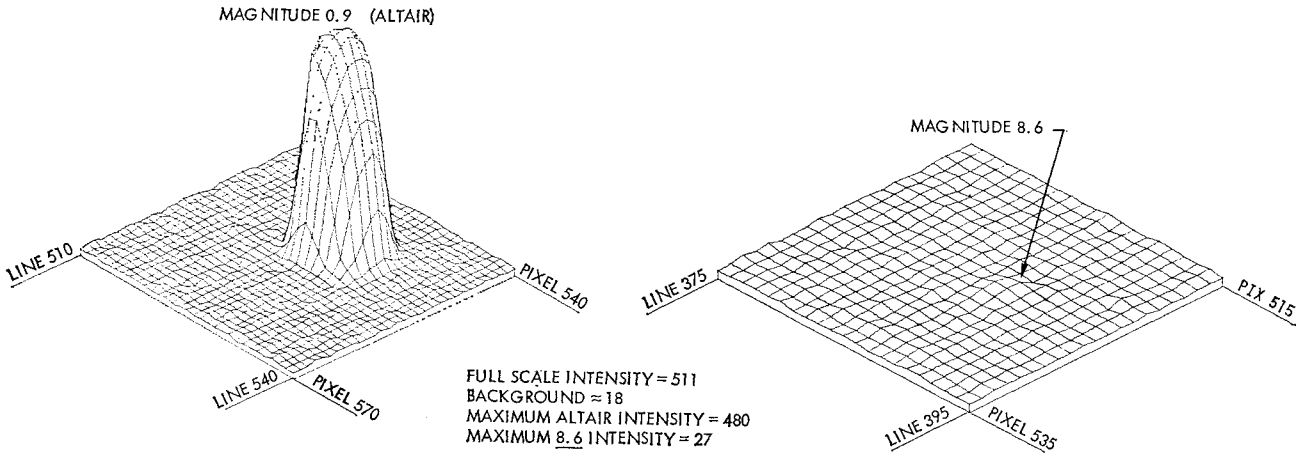

Fig. 5 Dynamic range of observed stars.

based on known camera pointing as obtained from spacecraft engineering telemetry. These overlays were used to help visually locate star images in photographic hard copy.

Video data returned from the spacecraft was intermixed with data from other science instruments in the telemetry stream. A two-stage computer program comprised of editing and scanning sections was used to process this data. Each video "record" consisted of one line of TV data, preceded by appropriate identification and status tags. Validation and sequence ordering of video records to produce complete digital representations of each TV picture was complicated by missing or duplicated records, bit errors in the TV line number and the occurrence of pseudovalid video data inserted in the data stream as a result of the stop-and-start transients of the spacecraft's tape recorder.

Initial plans for image detection assumed that celestially referenced TV pointing knowledge good to ± 25 pixels in each axis would be available prior to video playback. This knowledge would be obtained by processing spacecraft engineering telemetry containing scan platform gimbal angles and attitude reference data from the Sun and Canopus trackers. Experience with processing the calibration sequence pictures in this fashion revealed the inordinate amount of time required to insure the detection of at least 2 validated star images in each picture. A method was devised for searching an entire picture for star and satellite images, using no a priori data on expected location.

Detection of a star based on the signal level of a single pixel as compared to the local noise level would require a large signal-to-noise ratio. However, the occurrence of bit errors during transmission to earth causes hundreds of noise spikes to occur in each picture, thus eliminating any consideration of dependable and efficient single-pixel analysis. Stars as dim as magnitude 8.0 were seen to generally cause a noticeable signal level in two adjacent pixels; this became the basis for automatic image detection. Further signal processing would filter out more types of noise, but would substantially increase the computer time required to process the more than 500,000 video samples in each picture. A set of algorithms was found which would filter out most noise in an acceptable length of time.

The first algorithm detects 2 adjacent pixels on a given line with video intensity greater than a predetermined threshold. The second algorithm rejects high-frequency, high-amplitude noise appearing as numerous faint white dots in Fig. 8. A third algorithm requires a valid signal to exhibit a significant, local signal-to-noise ratio, thus allowing detection of a star substantially masked by stray light (Fig. 8), while rejecting the stray light itself. The fourth algorithm eliminates "re-detection" of a given signal when processing the next TV line. Some additional filtering is required to eliminate false signals caused by other peculiarities inherent in the data.

Each signal not rejected triggered a display of the local video data, centered at the location of the "detected" signal (Fig. 9). Each 20×20 pixel line printer display was visually examined by an analyst who (based on any available a priori information on expected star locations, an understanding of limit cycle motion and possible pointing errors, and a knowledge of the general characterization of star images, noise

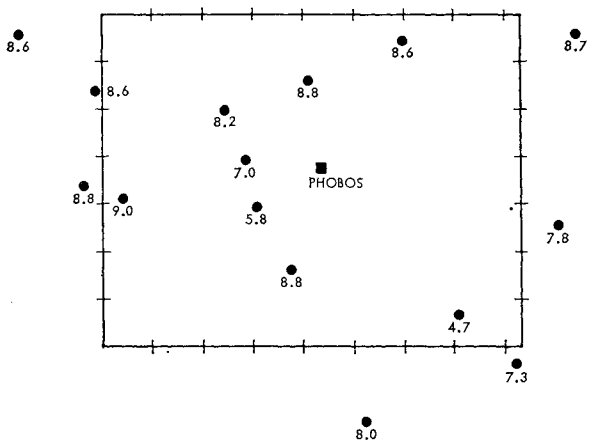

Fig. 6 Simulated TV picture.

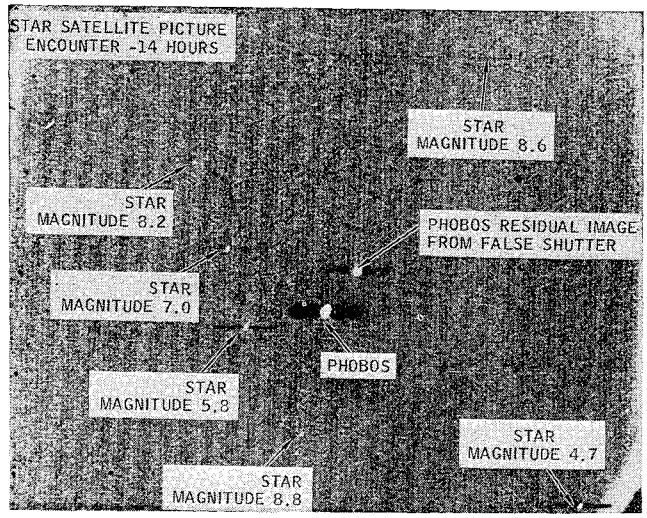

Fig. 7 Star-satellite picture at *E*-14 hr.

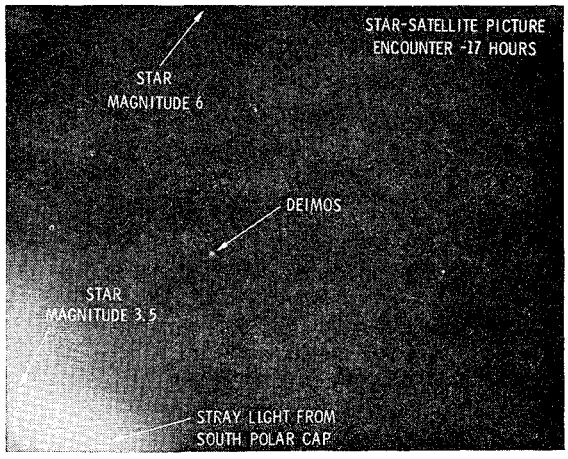

Fig. 8 Star-satellite picture showing high frequency and broad-band noise.

spikes and vidicon target blemishes) would accept or reject each signal as representing a valid image. Figure 10 shows a video intensity plot corresponding to the data listed in Fig. 9. The star of magnitude 8.1 produced a peak signal very nearly the same as that of the nearby noise spike. Selection of this noise as corresponding to the star image could lead to a pointing error of up to 48 arc sec.

Image center location was degraded by image blooming, image trailing, vidicon-beam deflection and point-spread effects. Blooming of about 5 pixels was observed for a moderately bright star (magnitude 4.6), and an image of Phobos subtending 4 pixels produced a substantial signal in 20 pixels (Fig. 11). Image trailing, caused by spacecraft limit cycle motion, was usually not noticeable. However, trailing of about 8 pixels was observed in one of the 21 approach sequence pictures, shown here in the image of a star of magnitude 6.2 (Fig. 12). Beam deflection and point-spread function tended to bias the peak output signal in the low-line/low-pixel direction. This effect is shown in Fig. 13, where equal intensity contours are plotted for a star of magnitude 6.9. With practice obtained by processing the calibration sequence pictures, the analyst tried to account for these effects when selecting exact-image locations.

Optical data rectification could be performed once the required spacecraft engineering data and observed image locations were available. The engineering telemetry, containing limit-cycle position and scan-platform pointing, was used for a priori camera orientation in the correlation of observed star image locations with expected locations. Star images were used to complete the pointing estimation, and the image location of Deimos or Phobos was corrected for distortion errors. The corrected satellite image location and associated observation statistics, along with the associated partial derivatives and the expected position of the satellite image based

	PIXEL									
	520							525		
380	16	16	16	17	18	16	16	12	12	18
	17	17	57	23	18	14	10	18	17	19
LINE	19	18	16	19	14	17	29	36	15	19
	18	15	14	19	12	20	44	(68)	35	19
	19	19	16	20	18	17	25	47	33	23
385	18	17	21	13	18	18	18	19	16	23

Fig. 9 Computer line printer display of video data.

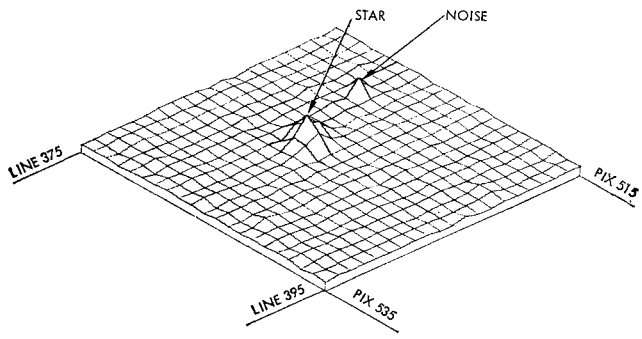

Fig. 10 Star (magnitude 8.1) and noise spike.

on the best estimate of the spacecraft state, were delivered to the mission navigation programs for combination with radio-tracking data prior to trajectory estimation.

System Performance

Eighteen pictures of Deimos and 3 pictures of Phobos were obtained during Mars approach. Six-second exposures were used for all pictures to maximize the number of detectable star images. The satellite image and at least 2 star images were found in each of 19 pictures within one hour of receipt of the raw video data (the remaining 2 pictures showed Phobos in transit across Mars). The spacecraft trajectory estimates obtained using varying amounts of optical and radio data proved to be extremely accurate, and provided nearly independent verification of radio-tracking estimates.[7]

The success of preinsertion satellite pictures was instrumental in decisions to attempt in-orbit imaging of Phobos and Deimos. The planning program used during approach was used in an alternate mode to identify good viewing opportunities. The excellent camera-pointing calibration effected prior to insertion was valuable in obtaining and analyzing close-range pictures. Aside from their scientific value, these pictures were used to update Phobos' and Deimos' ephemerides. Since no stars were visible (exposures were not more than 48 msec) the calibrated spacecraft math models allowed a posteriori camera-pointing accuracy of 0.017° (1σ), using the spacecraft celestial attitude sensors (Sun and Canopus) for reference.

Conclusions

The combination of vidicon sensitivity, camera field of view and spacecraft limit cycle rates obtained with the Mariner 9 spacecraft proved to be sufficient for obtaining the required

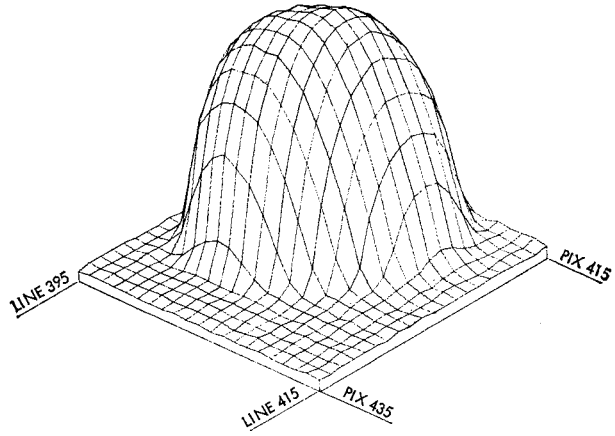

Fig. 11 Phobos image.

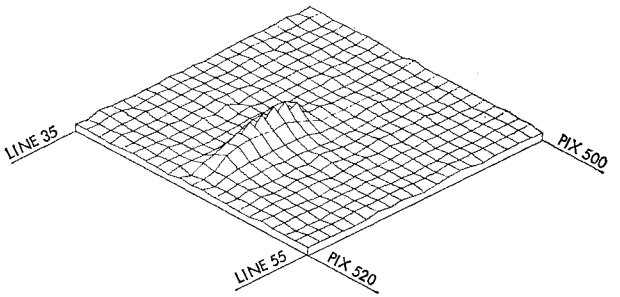

Fig. 12 Star image showing trailing.

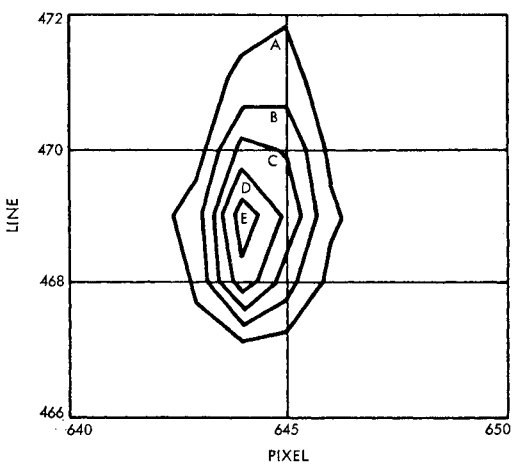

ARC LABEL	CONTOUR VALUE
A	20
B	30
C	40
D	50
E	60

Fig. 13 Video contour plot of 6.9 magnitude star.

images to produce reliable optical navigation observations. In-flight calibration of spacecraft and TV error models was an integral part of the experiment, allowing a high degree of accuracy and confidence in the results obtained, and providing invaluable operational experience with real data. The software required during Mars encounter was considerably more complex than originally designed. Future systems must make extensive use of real-time, interactive programs and *I/O* devices. Complete or near-complete automation of data extraction, data editing and image identification will significantly reduce the time-critical trajectory-estimation process. New developments in vidicon and onboard computer technology may allow some amount of video data editing and /or compression prior to transmission to Earth. Such a calability may be essential for missions to the outer planets where data rates will be significantly less than the 16.2 killibits/sec achieved on Mariner 9. Extensive analysis of the data obtained during this mission will conclusively validate the use of star-satellite optical measurements combined with Earth-based radio tracking for navigation of interplanetary spacecraft.

References

[1] Kingsland, L., Jr., "Trajectory Analysis for a Grand Tour Mission to the Outer Planets," *Journal of Spacecraft and Rockets*, Vol. 6, No. 8, Aug. 1969, pp. 897–902.

[2] Ball, J. E. and Duxbury, T. C., "Navigating the Grand Tours," *Astronautics and Aeronautics*, Vol. 8, No. 9, Sept. 1970, pp. 73–76.

[3] Friedman, L. D., Hamilton, T. W., and Stanton, R. H., "Estimating Trajectory Correction Requirements for the Outer Planets Grand Tour Missions," AIAA Paper 72-54, San Diego, Calif., 1972.

[4] Duxbury, T. C., "A Spacecraft-Based Navigation Instrument for Outer Planet Missions," *Journal of Spacecraft and Rockets*, Vol. 7, No. 8, Aug. 1970, pp. 928–933.

[5] Duxbury, T. C. and Ohtakay, H., "In-Flight Calibration of an Interplanetary Navigation Instrument," *Journal of Spacecraft and Rockets*, Vol. 8, No. 10, Oct. 1971, pp. 1038–1042.

[6] Thorpe, T. E., private communication, June 1971, Jet Propulsion Lab., Pasadena, Calif.

[7] Duxbury, T. C. and Acton, C. H., "On Board Optical Navigation Data From Mariner '71," presented at the Institute of Navigation's National Space Meeting, Orlando, Fla., March 16, 1972.